ISSN 1330-3651 (Print), ISSN 1848-6339 (Online)
DOI: 10.17559/TV-20151217142924

SKEWED PRESSURE CHARACTERISTICS INDUCED BY STEP-BY-STEP EXCAVATION OF A DOUBLE-ARCH TUNNEL BASED ON INFRARED THERMOGRAPHY

Shu-ren Wang, Chun-liu Li, De-jian Li, Yan-bo Zhang, Paul Hagan

Original scientific paper
In order to obtain the skewed pressure characteristics, the physical model tests, adopting two kinds of excavation sequences of the bench method and the expanding method, were conducted under the different confining pressures for observation thermal radiation characteristics of the skewed pressure induced by step-by-step excavation for a double-arch tunnel. Firstly, under uniaxial compression test, the cylindrical specimen presented the cooling effect, the correlations between the axial stress of the cylindrical specimen and its surface thermal radiation temperature displayed negative nonlinear correlation in the pre-peak curve and linear correlation in the post-peak curve, respectively. Secondly, for the physical model tests, the stress-temperature-time curves showed obvious two-phase trend as first moderate decline and then rapid decline stages, and the latter was slower than the former for an excavation step after all excavations being completed. The results showed that for two different excavation sequences, the failure positions on the vault of the double-arch tunnel due to being unloaded are diametrically opposed. Then the corresponding relationships between the skewed pressure induced by double-arch tunnel excavation and the temperature field of the infrared thermal radiation were revealed, which can provide a reference for the reasonable excavation and security support of the double-arch tunnel.

Keywords: *double-arch tunnel; excavation; infrared radiation; physical model; skewed pressure*

Značajke asimetričnog tlaka induciranog postupnim iskapanjem tunela s dvostrukim svodom na osnovu infracrvene termografije

Izvorni znanstveni članak
U svrhu dobivanja značajki asimetričnog tlaka provedena su ispitivanja fizičkog modela, primjenom dviju vrsta nizova iskopavanja metode etaže i metode širenja, kod tlaka različitog ograničenja za promatranje značajki toplinskog zračenja asimetričnog tlaka induciranog postupnim iskapanjem tunela s dvostrukim svodom. Najprije, kod jednoosnog ispitivanja na pritisak, cilindrični uzorak je predstavljao učinak hlađenja, a korelacije između aksijalnog naprezanja cilindričnog uzorka i njegove temperature zračenja na površini pokazale su negativnu nelinearnu korelaciju u krivulji prije vršnog naprezanja i linearnu korelaciju krivulje nakon vršnog naprezanja. Zatim, za ispitivanje fizičkog modela, krivulje naprezanje-temperatura-vrijeme pokazivale su očiti dvofazni trend kao najprije umjereni otklon, a zatim stadije rapidnog otklona, koji su bili slabiji od prethodnih za jedan korak iskapanja nakon završetka svih iskapanja. Rezultati su pokazali da su za dva različita slijeda iskapanja, mjesta kvara na svodu tunela nastala zbog rasterećenja, dijametralno suprotna. Tada su otkriveni i odgovarajući odnosi između asimetričnog tlaka nastalog iskapanjem tunela s dva svoda i temperaturnog polja infracrvenog toplinskog zračenja, što može biti preporuka za razumno iskopavanje i veću sigurnost tunela s dva svoda.

Ključne riječi: *asimetrični tlak; fizički model; infracrveno zračenje; iskapanje; tunel s dvostrukim svodom*

1 Introduction

The infrared radiation imaging technology, using the infrared radiation principle to convert the infrared radiation temperature distribution of the surface into an infrared image, characterizing non-contact, real-time and full-range of features, can obtain the completely temporal and spatial information of stress-field of the material surface. Therefore, it was of an important application value in the practical engineering [1÷3].

In recent years, the thermal radiation imaging (TIR) technology in several countries has been widely applied to various aspects. For example, Etoa et al. examined the infrared radiation properties and surface characteristics of carbon-carbon compopoints and graphites from the viewpoint of the nondestructive detection of defects in these materials, and they found that the larger the pore size and roughness of specimen, the larger the variation of data points [4]. Ploteau et al. aimed at presenting the development, the construction, the calibration, and the test of flux meters designed to make in situ measurements of infrared radiation in industrial furnaces [5]. In order to have the distinct spectral features, Balick et al. used an hyperspectral imaging spectrometer measuring in the longwave thermal infrared in the field to observe the variability of emissivity spectra of individual rock surfaces [6]. Park applied the thermal infrared camera to detect the increase of temperature and the distribution of thermal abnormalities before and after failure under uniaxial loading, for the granite, diorite, basalt and tuff specimens obtained in Korea [7]. Baron et al. presented a new approach for mapping open cracks and tension fractures within rock slope instabilities and rock cliffs, which resided in high-resolution ground-based and airborne infrared thermography [8]. Usamentiaga et al. presented a general introduction to infrared thermography and the common procedures for temperature measurement and non-destructive testing [9]. Manuel et al. conducted the possibilities of the use of IR thermography in rotating tool processes such as milling [10].

So far, China has also made quite a number of important achievements in research of thermal radiation technology. For example, based on TIR detection during uniaxial loading of rock samples, Wu et al. found the TIR-anomaly characteristics of the rock surface reflect the features of rock deformation or rock failure [11]. Li et al. discussed the main characteristics of infrared radiation thermography on temperature measurement and the development of infrared thermographic equipments. They also reviewed the applications of infrared thermographic techniques, thermal diagnosis of equipments, testing of structures and buildings, and prevention and cure of disasters [12]. Zhang et al. conducted the research on TIR with rock deformation of tunnel without bolts and bolted tunnel in the process of confined compressions. They found that the TIR temperature of the bolted tunnel wall

rock increased higher and changed more rapidly than that of tunnel wall rock without bolts, and that TIR is stronger in the location of stress concentration and bolted ranges than that in the location of stress relaxation and crushed ranges [13]. Based on the thermodynamics theory and physical micro-properties of solid materials subjected to external loading at room temperature, Wang et al. deduced a formula of calculating temperature difference of infrared radiation (IR) in terms of the sum of three principal strains to quantitatively investigate the infrared radiation characteristics in test [14]. He et al. simulated a roadway excavation in the geologically horizontal strata at great depth based on physical modeling test by using infrared thermography. The infrared thermography provided an enhanced understanding of the excavation response in terms of initiation, propagation and coalescence of rock damage in the spatial and frequency regimes respectively [15]. Chen et al. employed the equivalent material simulating experiments and thermal infrared imager equipments to study the rules of deformation and failure of surrounding rock induced by rock burst [16]. Gong et al. conducted experiments on roadway excavation in large-scale geological physical models and captured the structural behavior of the differently inclined rock strata based on infrared thermographic technique [17]. Zhang et al. carried out an experiment to study the infrared radiation temperature characteristics of granites under different moisture conditions by using infrared thermal imager [18].

In a word, the infrared radiation imaging technology as a method of observation of the material surface temperature, was widely used in China and other countries and many research results had been achieved. However, the study of the infrared radiation characteristics of the skewed pressure during the double-arch tunnel excavation, together with considering the pressure conditions and excavation sequences of a double-arch tunnel, is rarely reported. Therefore, the similar material model tests were carried out for observation of thermal radiation characteristics of the skewed pressure induced by step-by-step excavation of a double-arch tunnel based on the infrared thermography. Furthermore, the corresponding relationships between the skewed pressure and the thermal radiation temperature field were revealed during the double-arch tunnel excavation. The results would provide the technical basis for reasonable excavation and security support of a double-arch tunnel.

2 Materials and methods

2.1 Test specimens

The typical dimensions of the double-arch tunnel were shown in Fig. 1a. The square plate for double-arch tunnel model, whose dimensions were length × height × thickness = 150 mm × 150 mm × 30 mm, was shown in Figure 1b. The white cement was selected as the similar material with the water-cement ratio of 0,8:1. And the same material standard cylindrical sample of diameter 50 mm and length 100 mm was made, with two ends being polished and the tolerance of parallelism less than 0,01 mm. The physical and mechanical parameters of the specimens were shown in Tab. 1.

2.2 Laboratory equipment

The loading device whose maximum load for 3000 kN was equipped with RLW-3000 servo control compression testing machine, as shown in Fig. 2. The biaxial testing machine was controlled by setting the displacement velocity to 0,0025 mm/s.

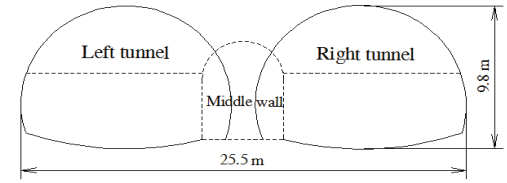

a) Typical dimensions of the tunnel

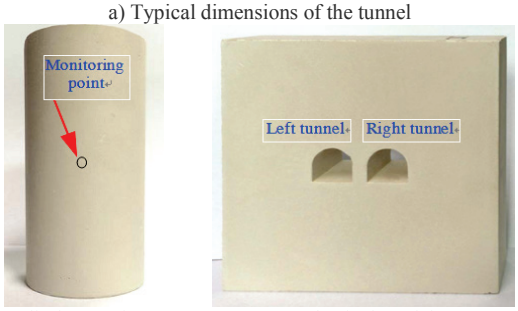

b) Cylinder specimen c) Physical model

Figure 1 Typical dimensions and physical model of the double-arch tunnel.

Table 1 Physical and mechanical parameters of the model.

Density (g/m^3)	Elastic modulus (GPa)	Poisson ratio	Water-cement ratio	Porosity (%)
0,941	1,67	0,23	0,8:1	65,35
Note	Cylindrical specimen: Diameter × length = 50 × 100 mm^2; Square plate with holes: Length × height × thickness = 150 × 150 × 30 mm^3.			

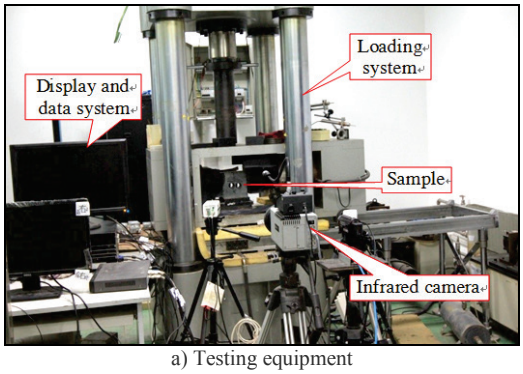

a) Testing equipment

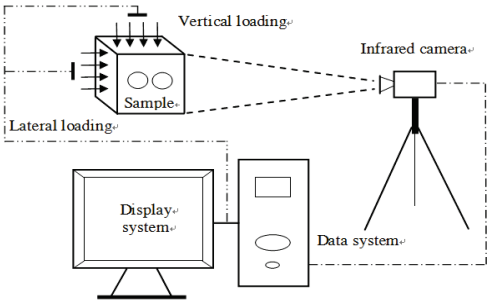

b) Scheme of testing system

Figure 2 Testing equipment and testing system layout.

A modern TIR imaging system, FLIR ThermaCAM SC3000 with temperature precision of 0,02 °C was applied for the TIR radiation detection and image

recording during the step-by-step excavation of double-arch tunnel. The infrared camera with 7,5 to 13 μm spectral response range was performed with the given calibration temperature within the range of −40 to +500 °C, and the IR image resolution was for 640 × 480 pixels.

2.3 Experimental procedures

The laboratory tests were conducted according to the following procedures:

(1) Turned on the computer, then started the devices, checked and debugged the mechanical testing system.

(2) Connected the infrared acquisition equipment of FLIR ThermaCAM SC3000 and debugged the corresponding devices.

(3) Placed the specimen just below the indenter, first made the indenter close to the specimen with a coarse control, then approximated the test specimen and loaded in accordance with the designed loading rate. The laboratory test was conducted according to the following procedures.

(4) The cylindrical specimens were loaded in the vertical direction at a constant rate of 0,0025 mm/s until the failure occured. The force and deformation of the specimens were monitored during the loading process.

(5) The physical model was loaded up to 7,5 kN in the biaxial direction at a constant rate 0,0025 mm/s firstly, then to 9,0 kN after the stabilization of 1.0 minute.

(6) As shown in Fig. 3, the bench method and the expanding method were adopted for the step-by-step excavation in the experiment respectively. When all the excavations were completed, the loading was continued until the specimen failed. AR01, AR02 and AR03 were the monitoring points of the infrared temperature.

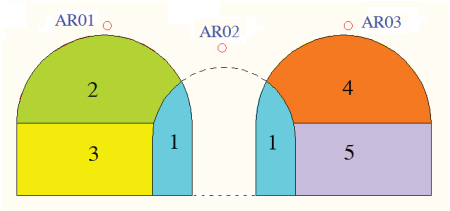

a) The bench method

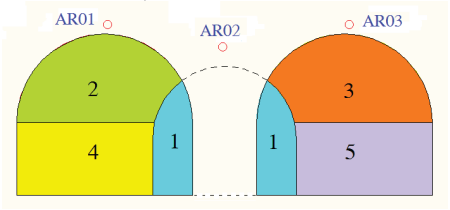

b) The expanding method

Figure 3 Step-by-step excavation sequences of the double arch tunnel.

(7) When the experiments were completed, at first the loadings in the horizontal direction and then in the axial direction were unloaded, uplifting the indenter, deriving the experimental data, removing the test specimen, and finally closing the related experimental equipment.

3 Results and discussions

3.1 Characteristics of stress-temperature-time curves of cylindrical sample

The average infrared radiation temperature (T_{AIR}) of the specimen surface, reflecting the infrared radiation energy of the entire specimen, is an important indicator to characterize the infrared radiation variation of the specimen in the loading process. The T_{AIR} of the specimen front surface (at a front view) was captured by IR camera in the test and the T_{AIR}-time curve was plotted. The uniaxial compressive stress-time curve is important to reflect the mechanical properties of the rock sample.

In the process of uniaxial loading tests, the cylindrical specimen stress-time curve experienced two-phase changes composed of a nonlinear rise until the peak value and then nearly a linear decline, and the stress-time curve showed larger fluctuations (Fig. 4a). The T_{AIR}-time curve of the cylindrical specimen showed a monotonically decreasing trend with time increasing, and the T_{AIR} dropped from 11.50 °C to 10,95 °C, the variation magnitude of the temperature was 0,55 °C.

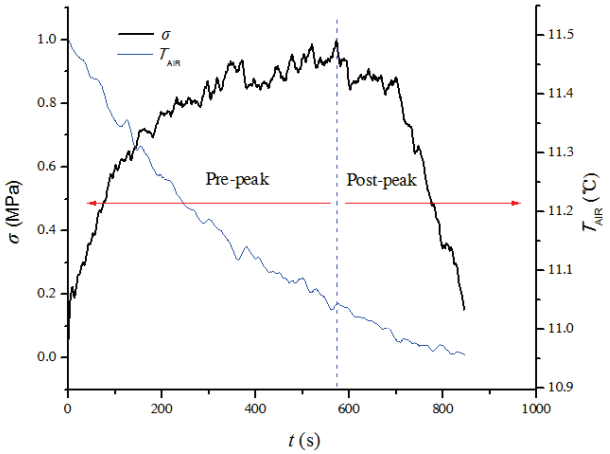

a) Stress-temperature-time curves

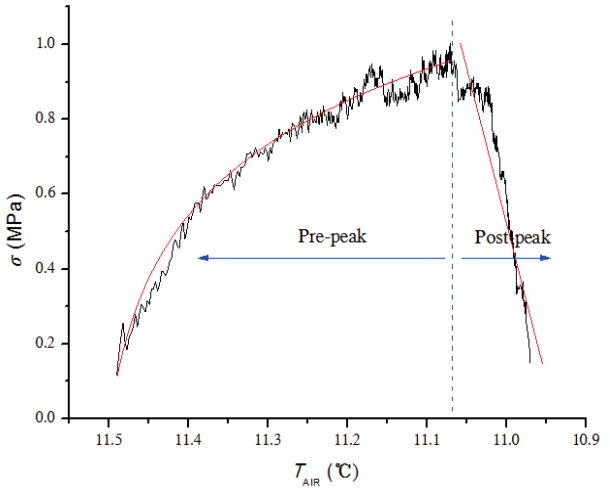

b) Stress-temperature curves

Figure 4 Stress-temperature-time and stress-temperature curves of the cylindrical specimen.

In order to reflect the infrared radiation characteristics of the sample under the uniaxial compression test, the relationship curves between the T_{AIR} and the axial stress of the sample were plotted. As seen from Fig. 4b, the relationships between the axial stress σ (MPa) and the average infrared radiation temperature t (°C) of the sample demonstrated a striking change with the load increasing, i.e. the negative nonlinear correlation in the front-peak phase and the linear correlation in the post-peak phase. The fitted equations were as follows:

$$\sigma = 11{,}50 - 0{,}0057 \cdot e^{\frac{t}{0{,}232}}, \text{ (Pre-peak phase)} \quad (1)$$

$$\sigma = 0{,}12 \cdot t + 10{,}94. \text{ (Post-peak phase)} \quad (2)$$

3.2 Characteristics of temperature and stress fields of the bench method

3.2.1 Characteristics of stress-temperature-time curves of the bench method

As shown in Fig. 5, the stress-temperature-time curves showed a downward trend as a whole with time. The second step excavation of the bench method was a critical step, before which the stress-temperature-time curves showed a moderate decline, after that the stress-temperature-time curves showed a rapid decline.

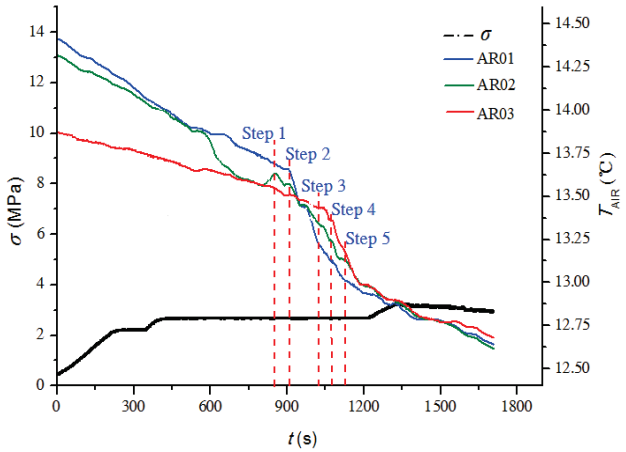

Figure 5 Stress-temperature-time variation curves of bench method.

When the first step excavation (840 s) of the double-arch tunnel was conducted, the temperatures of three monitoring points were t_{AR01} = 13,70 °C, t_{AR02} = 13,62 °C and t_{AR03} = 13,54 °C, namely $t_{AR01} > t_{AR02} > t_{AR03}$.

When the second step excavation (905 s) was conducted, the temperatures of three monitoring points were t_{AR01} = 13,66 °C, t_{AR02} = 13,56 °C and t_{AR03} = 13,50 °C, namely $t_{AR01} > t_{AR02} > t_{AR03}$. According to Eq. (1), the stresses of the surrounding rock of the double arch tunnel were $\sigma_{AR01} < \sigma_{AR02} < \sigma_{AR03}$.

When the third, the fourth or the fifth step excavations were carried out, the temperature curves of three monitoring points showed the rapid downward trend, indicating that the surrounding rock of the tunnel was in a stress relaxation or a plastic deformation stage. Due to the temperatures of three monitoring points were $t_{AR03} < t_{AR02} < t_{AR01}$, according to Eq. (2), the stresses of the surrounding rock of the double arch tunnel were $\sigma_{AR01} < \sigma_{AR02} < \sigma_{AR03}$.

3.2.2 Characteristics of IR image of the bench method

The timing sequence of the double-arch tunnel excavation and the surface infrared image changes of the bench method were shown in Figs. 6 and 7, respectively.

The second step excavation was a critical step, before which the surrounding rock of the double-arch tunnel was in an elastic deformation stage, after that the failure appeared in the vault of the left tunnel (Fig. 6c), indicating that the surrounding rock of the tunnel was in a stress relaxation or a plastic deformation stage.

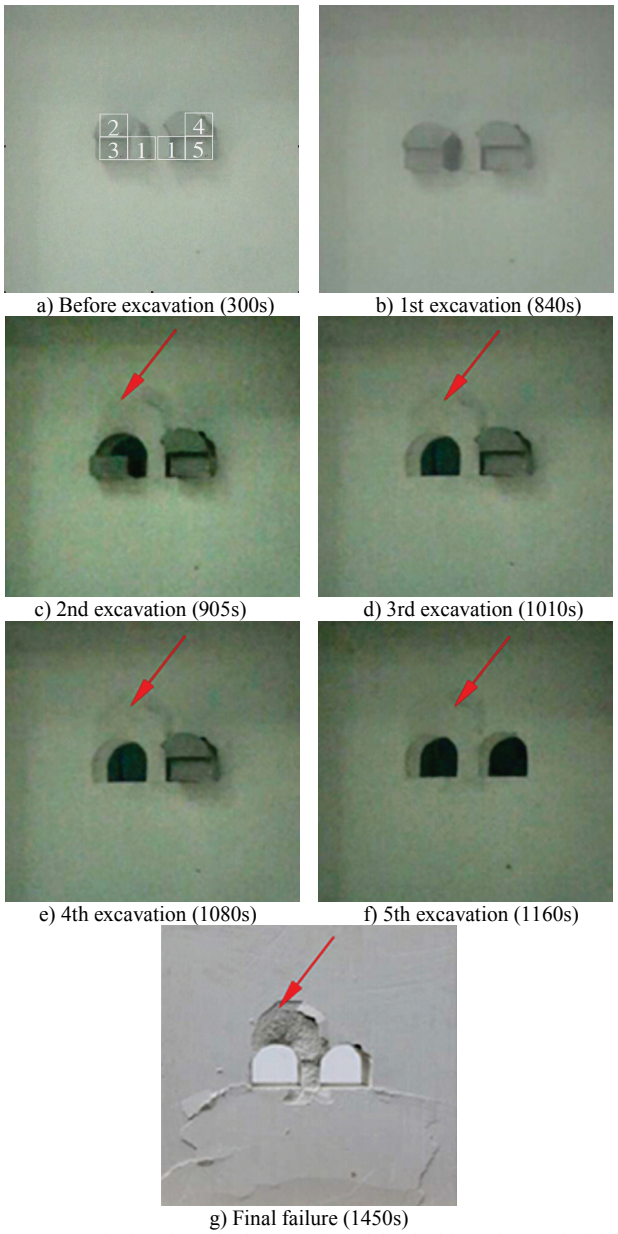

a) Before excavation (300s) b) 1st excavation (840s)

c) 2nd excavation (905s) d) 3rd excavation (1010s)

e) 4th excavation (1080s) f) 5th excavation (1160s)

g) Final failure (1450s)

Figure 6 The bench method excavation of the double-arch tunnel with different time.

It could be seen from Fig. 7 that corresponding to the excavation sequence, the infrared image colors of the specimen surface underwent the changes from warm to cool, which were consistent with the results from the infrared radiation temperature–time curves of the monitoring sites.

3.3 Characteristics of temperature and stress fields of the expanding method

3.3.1 Characteristics of stress-temperature-time curves of the expanding method

As shown in Fig. 8, the stress-temperature-time curves showed a downward trend as a whole with time increasing. The third step excavation of the double-arch tunnel is a critical step, before which the stress-temperature-time curves showed a moderate decline, after

that the stress-temperature-time curves showed a rapid decline.

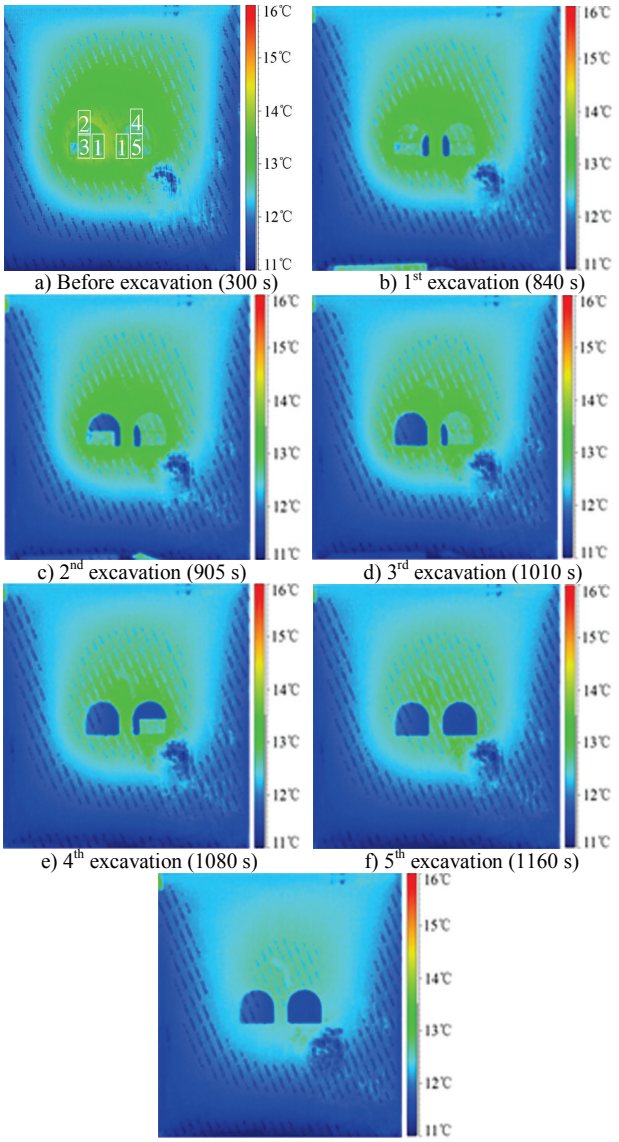

a) Before excavation (300 s) b) 1st excavation (840 s)
c) 2nd excavation (905 s) d) 3rd excavation (1010 s)
e) 4th excavation (1080 s) f) 5th excavation (1160 s)
g) Final failure (1450 s)

Figure 7 IR images of the bench method excavation with different time.

When the first step excavation (480 s) was conducted, the temperatures of three monitoring sites were t_{AR01} = 12,20 °C, t_{AR02} = 12,28 °C and t_{AR03} = 12,15 °C, respectively. When the second step excavation (545 s) was conducted, the temperatures of three monitoring sites were t_{AR01} = 12,19 °C, t_{AR02} = 12,26 °C and t_{AR03} = 12,14 °C, respectively. After the third step excavation, the temperatures of three monitoring points were t_{AR01} = 12,11 °C, t_{AR02} = 12,08 °C and t_{AR03} = 12,13 °C, respectively. According to Eq. (1), the stresses of the surrounding rock of the double arch tunnel were $\sigma_{AR03} < \sigma_{AR01} < \sigma_{AR02}$.

When the fourth and the fifth step excavations were carried out, the temperature curves of three monitoring sites showed a rapid downward trend, indicating that the surrounding rock of the tunnel was in the stress relaxation or plastic deformation stage. Due to the temperatures of three monitoring points being $t_{AR02} < t_{AR01} < t_{AR03}$, according to Eq. (2), the stresses of the surrounding rock of the double arch tunnel were $\sigma_{AR02} < \sigma_{AR01} < \sigma_{AR03}$.

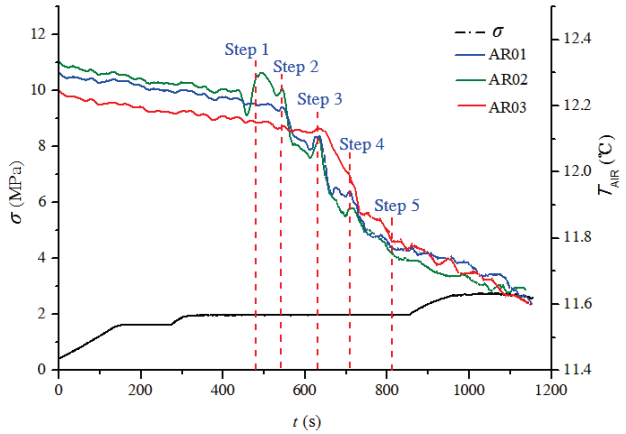

Figure 8 Stress-temperature-time variation curves of the expanding method.

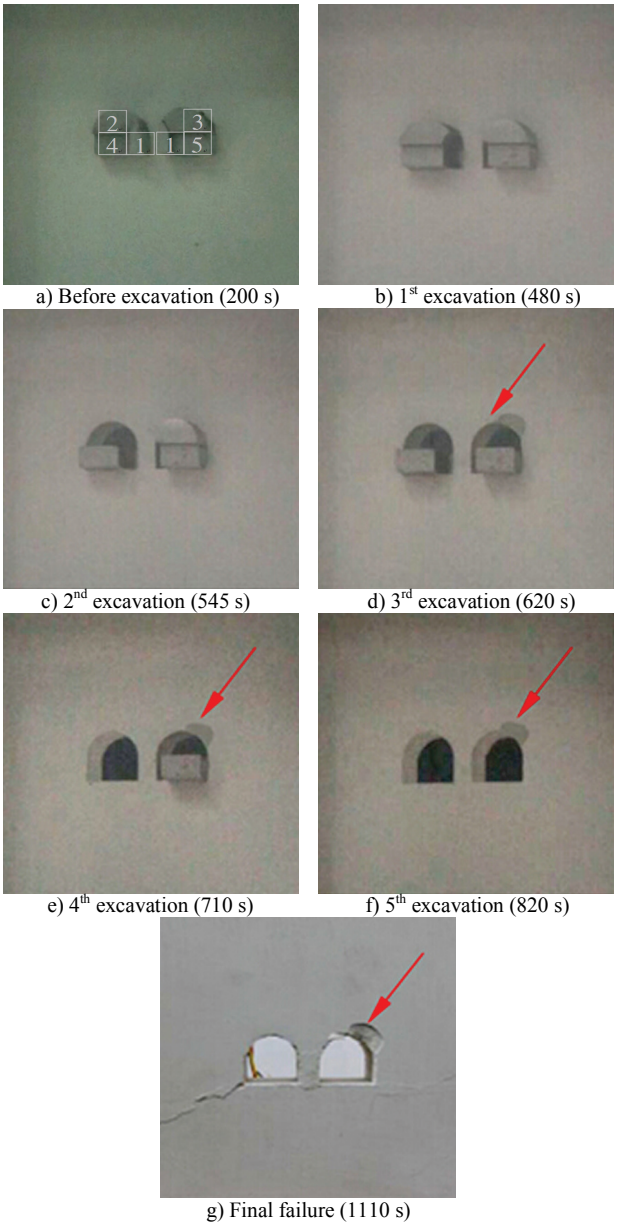

a) Before excavation (200 s) b) 1st excavation (480 s)
c) 2nd excavation (545 s) d) 3rd excavation (620 s)
e) 4th excavation (710 s) f) 5th excavation (820 s)
g) Final failure (1110 s)

Figure 9 The expanding method excavation of the double-arch tunnel with different time.

3.3.2 Characteristics of IR image of the expanding method

The timing sequence of the double-arch tunnel excavation and the surface infrared image changes of the

expanding method were shown in Figs. 9 and 10, respectively.

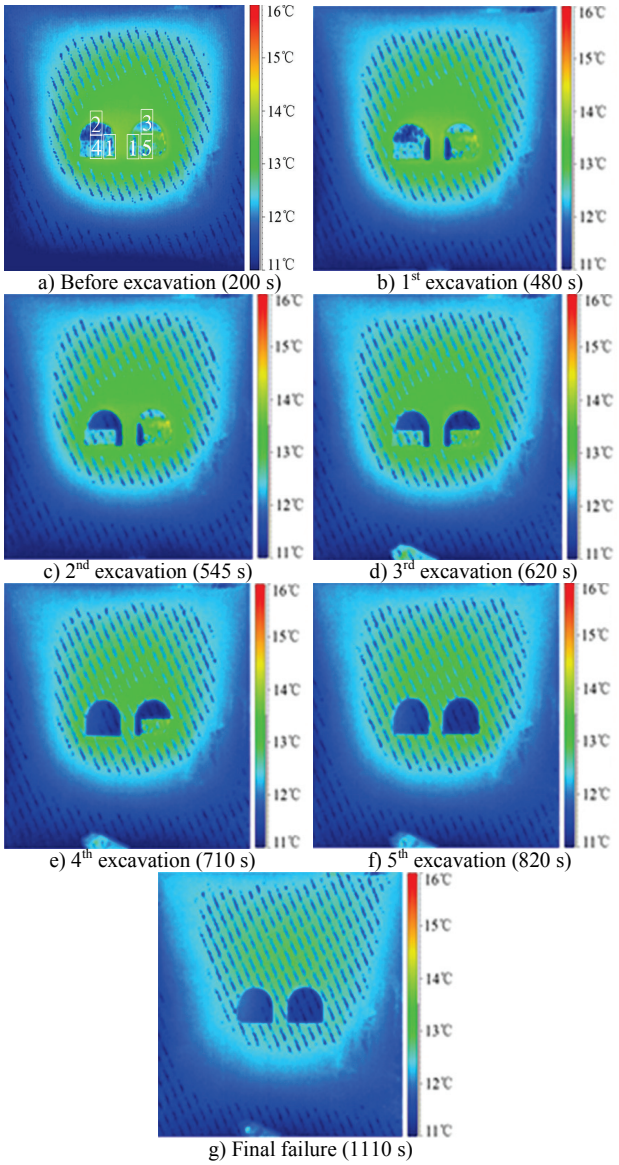

Figure 10 IR images of the expanding method excavation with different time.

The third excavation step was a critical step, before which the surrounding rock of the double-arch tunnel was in the elastic deformation stage, after that as a result of failure appeared in the vault of the right tunnel (Fig. 8d), indicating that the surrounding rock of the tunnel was in a stress relaxation or a plastic deformation stage.

It could be seen from Fig. 10 that corresponding to the excavation sequence, the infrared image colors of the specimen surface underwent the changes from warm to cool, which were consistent with the results derived from the infrared radiation temperature–time curves of the monitoring points.

4 Conclusions

The uniaxial stress-time curve experienced two-phase changes for a rise till peak value and then decline with time, and the stress-time curve showed larger fluctuations. The thermal radiation temperature-time curve showed a monotonically decreasing trend, and the cylindrical specimen displayed the cooling effect. The relationships between the axial stress and the average infrared radiation temperature of the sample demonstrated the negative nonlinear correlation in the pre-peak phase and the linear correlation in the post-peak phase.

By the bench method and the expanding method excavations of the double-arch tunnel, the stress-temperature-time curves showed two-stage trend composed of a moderate decline and a rapid decline stages with time, and the latter was slower than the former for an excavation step. Corresponding to the excavation sequence of two different excavation methods, the specimen surface colors of the infrared images underwent changes from warm to cool, which were consistent with the results derived from the infrared radiation temperature–time curves of the monitoring points.

Before the failure of the double-arch tunnel, the stresses of monitoring points at the top of the tunnel by the bench method excavation were the right tunnel, the middle rock pillar and the left tunnel in order of size. While the stresses of monitoring points at the top of the tunnel by the expanding method excavation were the middle rock pillar, the left tunnel and the right tunnel respectively. After the second step excavation by the bench method, the failure appeared in the vault of the left tunnel. While after the third step excavation by the expanding method, the failure appeared in the vault of the right tunnel.

The monitoring stresses were carried out from point information to field information during the step-by-step excavations of the double-arch tunnel by using the infrared thermography. The results in the paper changed so that we could not obtain the post-peak stress information due to material failure inducing the strain gauge peeling in the traditional way of point information monitoring stress. So the results in the paper are of important meaning to develop the infrared thermography to conduct the stress field monitoring.

5 Acknowledgments

This work was financially supported by the National Natural Science Foundation of China (51474188; 51074140; 51310105020), the Natural Science Foundation of Hebei Province of China (E2014203012), 2015 Endeavor Research Fellowship and Program for Taihang Scholars, all these are gratefully acknowledged. We also thank teachers and graduate students such as Tian Baozhu, Liu Xiangxin, Liang Peng, Sun yong, Yu Guangyuan, Liu Cuiping, Xu Jipeng and Wei Haiming for their indispensable assistances during the tests.

6 References

[1] Tan, Z. H.; Tang, C. A.; Zhu, W. C.; Wang, S. Y.; Chen, Z. H. Experimental study on infrared thermal image for failure process of granite with fracture. // Chinese Journal of Rock Mechanics and Engineering. 24, 16(2005), pp. 2977-2981.

[2] Dehkordi, M. S.; Shahriar, K.; Maarefvand, P.; Nik, M. G. Application of the strain energy to estimate the rock load in non-squeezing ground condition. // Archives of Mining Sciences, 56, 3(2011), pp. 551-566.

[3] Thayammal, S.; Selvathi, D. A review on segmentation based image compression techniques. // Journal of

Engineering Science and Technology Review. 6, 3(2013), pp. 134-140.
[4] Etoa, M.; Ishiia, T.; Inagakib, T.; Okamotoc, Y. Infrared radiation properties of the carbon–carbon compopoint and their application to nondestructive detection of its defects. // Carbon. 40, 3(2002), pp. 285-294. DOI: 10.1016/S0008-6223(01)00094-X
[5] Ploteau, J. P.; Glouannec, P.; Noel, H. Conception of thermoelectric flux meters for infrared radiation measurements in industrial furnaces. // Applied Thermal Engineering. 27, 2-3(2007), pp. 674-681. DOI: 10.1016/j.applthermaleng.2006.05.010
[6] Balick, L.; Gillespie, A.; French, Ar.; Danilina, I.; Allard, J. P.; Mushkin, A. Longwave thermal infrared spectral variability in individual rocks. // Geoscience and Remote Sensing Letters, IEEE. 6, 1(2009), pp. 52-56. DOI: 10.1109/LGRS.2008.2006005
[7] Park, H. D. Investigation of rock failure under uniaxial loading using thermal infrared image. // Journal of the Korean Society of Mineral and Energy Resources Engineers. 47, 4(2010), pp. 505-514.
[8] Baron, I.; Beckovsky, D.; Mica, L. Application of infrared thermography for mapping open fractures in deep-seated rockslides and unstable cliffs. // Landslides. 11, 1(2014), pp. 15-27. DOI: 10.1007/s10346-012-0367-z
[9] Usamentiaga, R. E.; Venegas, P.; Guerediaga, J.; Vega, L.; Molleda, J.; Bulnes, F. G. Infrared thermography for temperature measurement and non-destructive testing. // Sensors. 14, 7(2014), pp. 12305-12348. DOI: 10.3390/s140712305
[10] Manuel, S. J. B.; Francisco, J. S. M.; Maria, D. P. T.; Roberto, L. R.; Oscar, M. L. Approach to the application of IR thermography in milling process study. // DYNA. 90, 2(2015), pp. 188-194.
[11] Wu, L. X.; Liu, S. J.; Wu, Y. H.; Wu, H. P. Changes in infrared radiation with rock deformation. // International Journal of Rock Mechanics and Mining Science. 39, 6(2002), pp. 825-831. DOI: 10.1016/S1365-1609(02)00049-7
[12] Li, G. H.; Wu, L. X.; Wu, M.; Qu, J. X. Current status and applications of infrared thermography. // Infrared and Laser Engineering, 33, 3(2004), pp. 227-230.
[13] Zhang, Y. J.; An, L. Q.; Ren, R. H.; Fan, S. M.; Ma, N. J.; Li, J. H.; Ji, Y. M.; Wang, J. Q. Experimental study of deformation of surrounding rock with infrared radiation. // Journal of China University of Mining & Technology, 15, 4(2005), pp. 329-333.
[14] Wang, F.; Li, Y. J.; Rao, Q. H.; Tang, L. Quantitative description of infrared radiation characteristics for solid materials subjected to external loading. // Journal of Central South University of Technology. 16, 6(2009), pp. 1022-1027. DOI: 10.1007/s11771-009-0169-1
[15] He, M. C.; Gong, W. L.; Zhai, H. M.; Zhang, H. P. Physical modeling of deep ground excavation in geologically horizontal strata based on infrared thermography. // Tunnelling and Underground Space Technology, 25, 4(2010), pp. 366-376. DOI: 10.1016/j.tust.2010.01.012
[16] Chen, Z. Q.; Zhang, Y. X.; Zhou, J. Y. Experimental study on infrared photographs of deformation and failure of surrounding rock of tunnels procession induced by excavation. // Chinese Journal of Geotechnical Engineering, 34, 7(2012), pp. 1271-1277.
[17] Gong, W. L.; Wang, J.; Gong, Y. X.; Guo, P. Y. Thermography analysis of a roadway excavation experiment in 60° inclined stratified rocks. // International Journal of Rock Mechanics and Mining Sciences, 60, (2013) pp. 134-147. DOI: 10.1016/j.ijrmms.2012.12.047
[18] Zhang, Y. B.; Li, J.; Liu, X. X.; Tian, B. Z.; Liu, S. J. Influence of water on infrared radiation characteristic of granite roadway rock burst. // Journal of Liaoning Technical University (Natural Science), 34, 4(2015), 453-458.

Authors' addresses

Shu-ren Wang, Ph.D., Professor
Corresponding author
1) School of Civil Engineering and Mechanics, Yanshan University,
No. 438 Hebei West Street, Haigang District, Qinhuangdao, 066004, China

2) Opening Laboratory for Deep Mine Construction, Henan Polytechnic University,
2001 Century Avenue, Jiaozuo, Henan Province, 454003, China
E-mail: w_sr88@163.com

Chun-liu Li, Ph.D. Candidate
1) School of Civil Engineering and Mechanics, Yanshan University,
No. 438 Hebei West Street, Haigang District, Qinhuangdao, 066004, China

2) Institute of Urban Construction, Hebei Normal University of Science & Technology,
No. 360 Hebei West Street, Haigang District, Qinhuangdao, 066004, China
E-mail: lclcc_010@163.com

De-jian Li, Ph.D., Associate Professor
State Key Laboratory for Geomechanics and Deep Underground Engineering, China University of Mining and Technology,
Ding No. 11 Xueyuan Road, Haidian District, Beijing 100083, China
E-mail: lidj@cumtb.edu.cn

Yan-bo Zhang, Ph.D., Professor
College of Mining Engineering, North China University of Science and Technology,
No. 46 Xinhua West Road, Tangshan, 063009, China
E-mail: fzdn44444@163.com

Paul Hagan, Ph.D., Associate Professor
School of Mining Engineering, University of New South Wales,
Gate 14, Barker Street, Sydney, 2052, Australia
E-mail: p.hagan@unsw.edu.au